

# P2RBox: A SINGLE POINT IS ALL YOU NEED FOR ORIENTED OBJECT DETECTION

Guangming Cao<sup>1\*</sup>, Xuehui Yu<sup>1\*</sup>, Wenwen Yu<sup>1</sup>, Xumeng Han<sup>1</sup>, Xue Yang<sup>2</sup>

Guorong Li<sup>1</sup>, Jianbin Jiao<sup>1</sup>, Zhenjun Han<sup>1†</sup>

<sup>1</sup>University of Chinese Academy of Sciences    <sup>2</sup>Shanghai Jiao Tong University

caoguangming21@mails.ucas.ac.cn

## ABSTRACT

Oriented object detection, a specialized subfield in computer vision, finds applications across diverse scenarios, excelling particularly when dealing with objects of arbitrary orientations. Conversely, point annotation, which treats objects as single points, offers a cost-effective alternative to rotated and horizontal bounding boxes but sacrifices performance due to the loss of size and orientation information. In this study, we introduce the P2RBox network, which leverages point annotations and a mask generator to create mask proposals, followed by filtration through our Inspector Module and Constrainer Module. This process selects high-quality masks, which are subsequently converted into rotated box annotations for training a fully supervised detector. Specifically, we’ve thoughtfully crafted an Inspector Module rooted in multi-instance learning principles to evaluate the semantic score of masks. We’ve also proposed a more robust mask quality assessment in conjunction with the Constrainer Module. Furthermore, we’ve introduced a Symmetry Axis Estimation (SAE) Module inspired by the spectral theorem for symmetric matrices to transform the top-performing mask proposal into rotated bounding boxes. P2RBox performs well with three fully supervised rotated object detectors: RetinaNet, Rotated FCOS, and Oriented R-CNN. By combining with Oriented R-CNN, P2RBox achieves 62.26% on DOTA-v1.0 test dataset. As far as we know, this is the first attempt at training an oriented object detector with point supervision.

## 1 INTRODUCTION

Aerial object detection focuses on identifying objects of interest, such as vehicles and airplanes, on the ground within aerial images and determining their categories. With the increasing availability of aerial imagery, this field has become a specific yet highly active area within computer vision (Ren et al., 2015; Lin et al., 2017; Tian et al., 2019; Ding et al., 2019; Xie et al., 2021).

Nevertheless, obtaining high-quality bounding box annotations demands significant human resources. Weakly supervised object detection (Bilen & Vedaldi, 2016; Tang et al., 2017; 2018; Chen et al., 2020; Wan et al., 2018; Zhou et al., 2016; Diba et al., 2017; Zhang et al., 2018) has emerged as a solution, replacing bounding box annotations with more affordable image-level annotations. However, due to the absence of precise location information and challenges in distinguishing densely packed objects, image-level supervised methods exhibit limited performance in complex scenarios. In recent times, point-based annotations have gained widespread usage across various tasks, including object detection (Papadopoulos et al., 2017; Ren et al., 2020), localization (Yu et al., 2022; Ribera et al., 2019; Song et al., 2021), instance segmentation (Cheng et al., 2022), and action localization (Lee & Byun, 2021).

One intriguing question naturally arises: Can weakly supervised learning for oriented object detection be achieved solely using point annotations instead of rotated bounding box annotations? We explore this question using a mask proposal generator (*e.g.*, SAM (Kirillov et al., 2023) as employed

\*Equal contribution.

†Corresponding author.

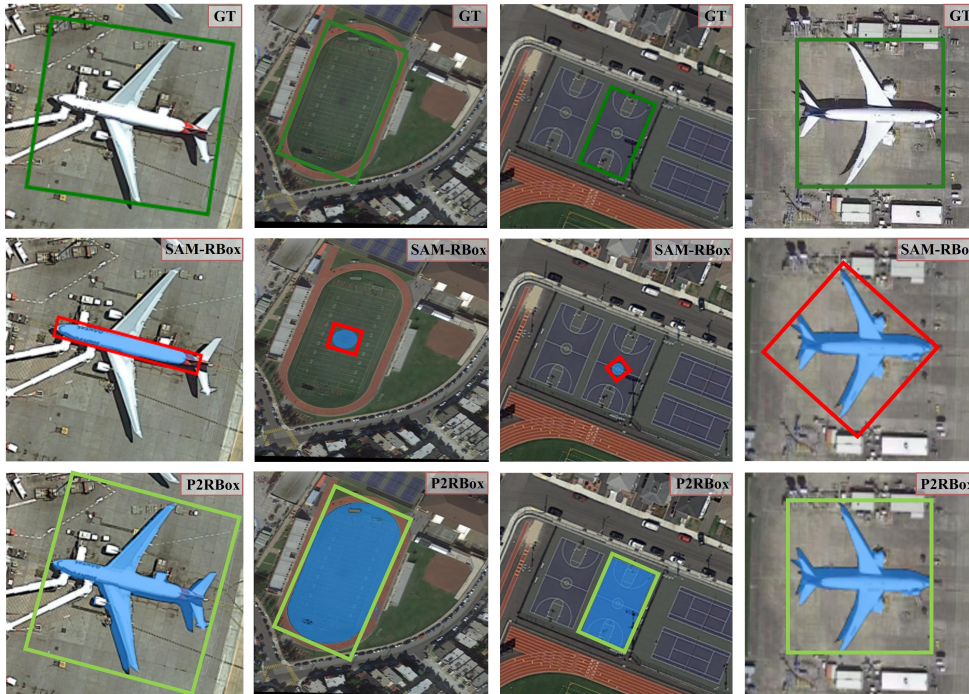


Figure 1: Visual comparison of the highest confidence mask and its corresponding rotated box annotation generated by mask proposal generator (SAM) and P2RBox. The second row displays the results of the baseline method, while the Rotated boxes in the last row are generated by the SAE module. (Best viewed in color).

in this paper). One straightforward approach is to choose the mask with the highest associated score as the object. Following this, we apply the minimum bounding rectangle method to transform it into rotated bounding box annotations, which serves as our baseline.

However, due to the lack of intra-class homogeneity, ambiguity arises between companion scores and the best-performing mask (the one with the highest Intersection over Union with the ground truth). This ambiguity leads to difficulties in selecting the best-performing mask based on companion scores, as illustrated in Fig. 1. In this paper, we introduce an architecture inspired by Multiple Instance Learning (MIL). By extracting mask proposal information during the Inspector Module, the network becomes proficient in classifying specific objects by aggregating information from annotated points across the entire dataset. This results in a semantic score that enhances the assessment of proposal masks. Additionally, we introduce the Constrainer Module, which takes into account the alignment between marked points and the center of gravity of a mask, providing offset penalties. After aggregating all these assessments, the best mask is selected using the new assessment criteria, and it is used to generate a rotated circumscribed bounding box via the Symmetry Axis Estimation (SAE) Module, as illustrated in Fig. 2. Our main contributions are as follows:

- 1) Proposing of the P2RBox Network: We introduce the P2RBox network, which is a method based on point annotation and a mask generator for achieving point-supervised rotated object detection. To the best of our knowledge, this marks the first attempt to train a rotated object detector using point supervision. By combining with Oriented R-CNN, P2RBox achieves 62.26% on DOTA-v1.0 test dataset.
- 2) High-Quality Mask Selection: Utilizing the Inspector Module, we introduce a semantic score for the masks, combined with the Constrainer Module, leading to the development of a comprehensive filtering approach. This, in turn, enhances the quality of the selected mask proposals from the mask generator and ultimately improves the quality of rotated bounding box annotations.
- 3) Mask-to-Rotated Box Conversion: We design the SAE module based on the spectral theorem for symmetric matrices to convert the best mask proposal into rotated bounding boxes, enhancing the effectiveness of rotated object detection.

## 2 RELATED WORK

**RBox-supervised Oriented Object Detection.** Notable approaches in this field include Rotated RetinaNet (Lin et al., 2017) with anchor-based methods, Rotated FCOS (Tian et al., 2019) using anchor-free techniques, and two-stage detectors like RoI Transformer (Ding et al., 2019), Oriented R-CNN (Xie et al., 2021), and ReDet (Han et al., 2021b). Performance enhancements have been seen with methods like R3Det (Yang et al., 2021b) and S2A-Net (Han et al., 2021a), leveraging alignment features. Most of these approaches use direct angle regression, but this can face challenges due to the periodic nature of angles, leading to strategies like modulated losses (Yang et al., 2019a; Qian et al., 2021), angle coders (Yang & Yan, 2020; Yang et al., 2021a; Yu & Da, 2023), and Gaussian-based losses (Yang et al., 2021c;d; 2022b;c). RepPoint-based approaches (Yang et al., 2019b; Hou et al., 2023; Li et al., 2022) provide alternative solutions for oriented object detection by predicting a set of sample points defining the object’s spatial extent.

**HBox-supervised oriented object detection.** While the oriented bounding box can be derived from the segmentation mask, employing the HBox-Mask-RBox pipeline can be less efficient in terms of cost. A pioneering approach, H2RBox (Yang et al., 2022a), bypasses the segmentation step and directly detects RBoxes from HBox annotations. By leveraging HBox annotations for the same object in various orientations, the geometric constraints narrow down the possible angles for the object, making the detection more efficient. Additionally, the integration of a self-supervised branch in H2RBox helps filter out undesirable results, establishing an HBox-to-RBox paradigm. In an extended version, H2RBox-v2 (Yu et al., 2023), a new self-supervised branch further enhances the precision of object angle learning, resulting in improved performance.

**Point-supervised object detection.** Point-level annotation, a recent advancement, is efficient, taking about 1.87 seconds per image on the VOC dataset (Everingham et al., 2010), comparable to image-level annotation (1.5 seconds per image) and much less than bounding box annotation (34.5 seconds per image), especially rotated bounding box annotation. However, the time for point-level annotation may increase with more objects in the image. P2BNet (Chen et al., 2022) uses a coarse-to-fine strategy, enhancing IoU with ground-truth by predicting pseudo boxes using point annotations and Faster R-CNN (Ren et al., 2015).

In a related context, (Yu et al., 2022) explores object localization with coarse point annotations, addressing point annotation’s semantic variability through algorithms. Additionally, (He et al., 2023) predicts horizontal bounding boxes in remote sensing scenes using point annotations. The Segment Anything Model (SAM) (Kirillov et al., 2023) allows obtaining object masks with a simple click, but ensuring mask quality remains challenging. Combining P2BNet (Chen et al., 2022) and H2RBox-v2 (Yu et al., 2023) provides the final object orientation, but H2RBox-v2 requires precise circumscribed horizontal bounding boxes. Background noise may affect both P2BNet and H2RBox-v2, leading to a poor performance (line of P2BNet-H2RBox in Tab. 1). Therefore, P2RBox focuses on generating high-quality rotated bounding boxes, a domain that has yet to be extensively studied to date.

## 3 POINT-TO-ROTATED-BOX NETWORK

As shown in Fig. 2, we design the P2RBox to establish a seamless connection between point annotations and rotated boxes through the generation, constraint, and inspection of mask proposals. Specifically, the annotated point located on an object serves as the prompt for producing initial mask proposals. Subsequently, a dedicated Constrainer Module is devised to discern and refine the most plausible masks. Building upon these filtered candidates, we introduce a novel Inspector Module designed to discern superior masks by intuitively capturing the semantic nuances embedded within the masks. Lastly, our improved mask-to-oriented-box module, named SAE, plays a pivotal component in facilitating the annotation transformation.

### 3.1 CONSTRAINER MODULE

In many cases, the annotated point of an object is typically positioned in close proximity to the center of the mask (Chen et al., 2022). Leveraging this observation, we introduce a penalty term that quantifies the distance between the mask’s center and the annotated point, thus facilitating the

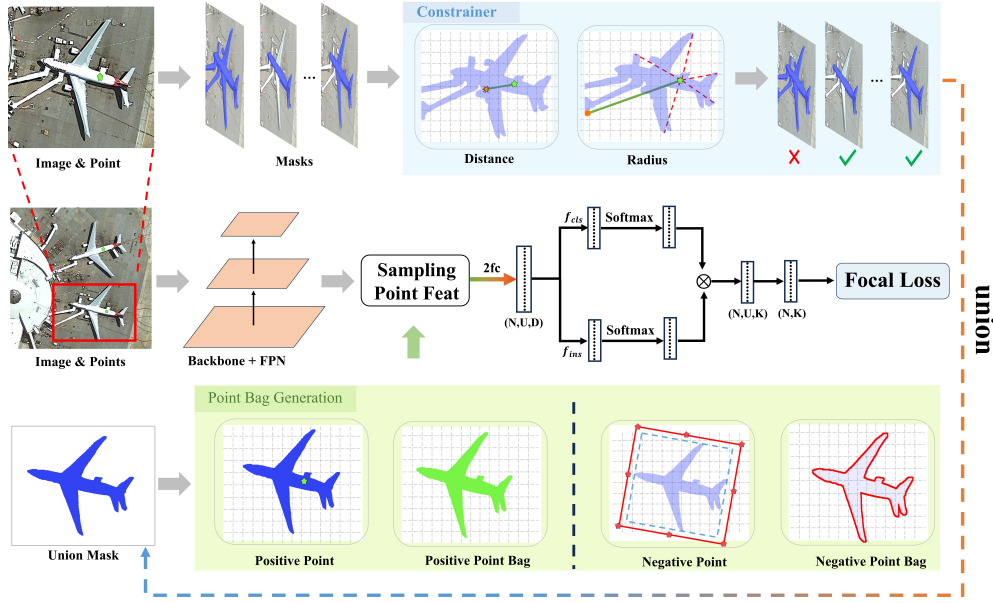


Figure 2: The overview of training process of P2RBox, consisting of mask generator, Constrainer Module and Inspector Module. Initially, mask proposals are generated by a generator (SAM). The Constrainer Module selects high-quality masks to create the union mask. Four point sets are constructed according the union mask to train Inspector Module, which pursuing dataset-wide category consistency. The trained network will be used to assess mask quality, selecting the best proposals for detector training supervision. (Best viewed in color)

prioritization of high-quality masks while effectively filtering out masks with excessive background content.

**Centroid Offset Penalty.** Let  $Radius$  represent the farthest Euclidean distance from any pixel on the mask to the annotation point, and  $dis$  denote the offset of the pixel’s centroid on the mask from the annotation point. A penalty formula regarding the relative offset is designed as follows:

$$S_{offset} = (1 - \exp(-w \cdot Radius + b)) \cdot \frac{dis}{Radius}. \quad (1)$$

While  $dis$  is scale-sensitive, we use  $dis/Radius$  to establish a scale-independent criterion. This approach works well for larger objects. However, consider small objects, we incorporate the term  $1 - \exp(-w \cdot Radius + b)$  to increase tolerance. This adjustment is necessary because even a single-pixel offset during annotation can result in significant changes. The term  $1 - \exp(-w \cdot Radius + b)$  ( $w$  set as 0.04,  $b$  set as 0.01, spectively) indicates that the coefficient is positively associated with the  $Radius$ . This suggests that the Constrainer operates under the assumption that as the  $dis/Radius$  ratio remains constant, a reduction in the value of  $Radius$  results in a corresponding decrease in  $S_{offset}$ . In our network, we only retain masks for which  $S_{offset}$  is less than the threshold  $thr1$ , set to 0.15 in our paper. During training, all masks meeting the criteria mentioned will be merged into a unified mask for subsequent steps.

### 3.2 INSPECTOR MODULE

Utilizing the qualified masks derived from the Constrainer Module, the Inspector Module samples positive and negative points to guide the model in acquiring deeper perception of the semantic category associated with specific objects, thereby enhancing the assessment of the proposal masks.

**Point Sampling.** The four points bag or set (positive bags, negative bags, negative points and annotation points.) are constructed to train inspector module, which are described here. We denote the coordinates of an annotated point as  $a \in \mathbb{R}^2$  and its corresponding category as  $c \in \{0, 1\}^K$ , where  $K$  represents the total number of categories.  $p = (p_x, p_y)$  denotes a point on a feature map.

**1) Positive Bag Construction.** In Fig. 2, with a relatively trustworthy mask in the neighborhood of  $a$ , we define  $Radius$  as the maximum Euclidean distance between the annotated point and pixels forming the mask. We define  $N$  ring-shaped sampling regions. Then we randomly sample  $u_0$  points within each region, and obtain  $Sample(a, r)$ . All sampled points of  $N$  ring-shaped regions are defined as points' bag of  $a$ , denoted as  $\mathcal{B}$  in Eq. 2.

$$Ring(a, r) = \{p | p \in mask, \frac{r-1}{N} < \frac{\|p-a\|}{Radius} \leq \frac{r}{N}, 1 \leq r \leq N\}. \quad (2)$$

$$Sample(a, r) = \{p_i | p_i \in Ring(a, r), p_i \text{ is randomly selected}\}. \quad (3)$$

$$\mathcal{B} = \bigcup_{1 \leq r \leq N} Sample(a, r), \quad (4)$$

where  $\mathcal{B}$  is used for calculating the MIL loss for P2RBox training, and  $|Sample(a, r)| = u_0$  ( $u_0$  are number of points sampled for each ring).

**2) Negative Bag Construction.** Background points located far from the object are easier for the network to learn. Conversely, the negative points along the object's boundary are more valuable samples, as they often reside on the critical boundary between the foreground and background. Hence, we design a negative point bag, training the model to discern boundary features. By selecting  $u_1$  points in the margin pixels of the mask, the negative point bag of  $a_j$  can be defined as:

$$\mathcal{B}_{neg} = \{p_i | p_i \in mask_{margin}, p_i \text{ is randomly selected}\}, \quad (5)$$

where  $|\mathcal{B}_{neg}| = u_1$  and  $mask_{margin}$  can be obtained by calculating the non-zero points on the gradient map (implemented using first-order differences) of the mask.

**3) Negative Points.** With annotated point  $a$  as a naturally positive reference, we introduce negative points to instruct the model in discerning background features. To obtain the negative points for a given mask, we follow a three-step process. Firstly, determine the circumscribed bounding box of the mask, denoted as  $(x, y, w, h, \alpha)$ . Secondly, increase both the height  $h$  and width  $w$  by a factor as  $\hat{h} = (1 + \delta) \cdot h$  and  $\hat{w} = (1 + \delta) \cdot w$ , where  $\delta$  is the set to 0.05 in this paper. Lastly, the set of negative points, denoted as  $\mathcal{N}$ , comprises the four vertices along with the midpoints of the four edges, *i.e.*,

$$n_{ij} = (x + \frac{\hat{w}}{2} \cdot \cos \alpha \cdot i - \frac{\hat{h}}{2} \cdot \sin \alpha \cdot j, y + \frac{\hat{w}}{2} \cdot \sin \alpha \cdot i + \frac{\hat{h}}{2} \cdot \cos \alpha \cdot j), \quad (6)$$

$$\mathcal{N} = \{n_{ij} | i, j \in \{-1, 0, 1\}, (i, j) \neq (0, 0)\}.$$

**P2RBox Loss.** In following, we gives the details of the objective function of training P2RBox network based on the positive bag  $\mathcal{B}$  and its score  $S_{\mathcal{B}}$ , negative bag  $\mathcal{B}_{neg}$  and its score  $S_{\mathcal{B}_{neg}}$ , and negative points  $\mathcal{N}$ . Based on the designed loss as described, after training, the network has acquired pixel-level classification capability.

**1) Bag Score.** To facilitate P2RBox in determining whether the points in  $\mathcal{B}$  belong to the same category as  $a$ , we treat the points in bag  $\mathcal{B}$  as positive instances. We extract the feature vectors  $\{\mathbf{F}_p | p \in \mathcal{B}\}$ . For each  $p \in \mathcal{B}$ , two separate fully connected layers with independent weights generate the classification score and instance score, denoted as  $[S_{\mathcal{B}}^{ins}]_p$  and  $[S_{\mathcal{B}}^{cls}]_p$ .

To obtain the final classification score for  $\mathcal{B}$ , we calculate it by summing the element-wise products of  $[S_{\mathcal{B}}^{ins}]_p$  and  $[S_{\mathcal{B}}^{cls}]_p$  as follows:

$$S_{\mathcal{B}} = \sum_{p \in \mathcal{B}} [S_{\mathcal{B}}^{ins}]_p \cdot [S_{\mathcal{B}}^{cls}]_p, \in \mathbb{R}^K. \quad (7)$$

This score will be used for the subsequent loss calculation.

**2) Total Loss.** Object-level MIL loss is introduced to endow P2RBox the ability of finding semantic points around each annotated point. By combining information from similar objects throughout the entire dataset, it imparts discriminative capabilities to the features of that category, distinguishing between foreground and background. The objective function of P2RBox is a weighted summation of the three losses:

$$\mathcal{L}_{P2RBox} = \mathcal{L}_{ann} + \mathcal{L}_{MIL}^{pos} + \mathcal{L}_{MIL}^{neg} + \mathcal{L}_{neg}. \quad (8)$$

And  $\mathcal{L}_{MIL}$ ,  $\mathcal{L}_{ann}$  and  $\mathcal{L}_{neg}$  are based on the focal loss (Lin et al., 2017):

$$\text{FL}(S_p, c) = \sum_{k=1}^K c_k (1 - S_{p,k})^\gamma \log(S_{p,k}) + (1 - c_k) S_{p,k}^\gamma \log(1 - S_{p,k}), \quad (9)$$

where  $\gamma$  is set as 2 following the standard focal loss.  $S_p \in \mathbb{R}^K$  and  $c \in \{0, 1\}^K$  are the predicted scores on all categories and the category label, respectively.

**3) Object-level MIL Loss.** As mentioned above,  $S_{\mathcal{B}}$  is computed for a set of points in bag  $\mathcal{B}$ . Each point’s classification score and instance score are generated independently. The final score is obtained by summing the element-wise products of these scores. Based on bag score  $S_{\mathcal{B}}$ , the MIL loss is given by the focal loss with the category label  $c$  of  $a$ :

$$\mathcal{L}_{MIL}^{pos} = \frac{1}{M} \sum_{j=1}^M \text{FL}(S_{\mathcal{B}_j}, c_j). \quad (10)$$

In a similar manner,  $\mathcal{L}_{MIL}^{neg}$  can be computed by applying the same procedure to  $\mathcal{B}_{neg}$ .

**4) Annotation Loss.** Due to the absence of positive samples with point annotations, the annotated points serve as natural positive samples that guide the model in learning about the foreground of each category. Hence, we introduce the annotation loss  $L_{ann}$  to provide the network with accurate positive samples for supervision.  $L_{ann}$  ensures a high score for annotated points. A classification branch with shared weights, as described above, is utilized to compute  $L_{ann}$  in the following manner.

$$S_a = \sigma(fc^{cls}(\mathbf{F}_a)) \in \mathbb{R}^K, \\ \mathcal{L}_{ann} = \frac{1}{M} \sum_{j=1}^M \text{FL}(S_{a_j}, c_j), \quad (11)$$

where  $M$  is the number of objects in an image,  $\sigma$  served as an activation function.

**5) Negative Loss.** Conventional MIL employs binary logarithmic loss and considers proposals from other categories as negative samples. Due to the absence of explicit supervision from background samples, it struggles to effectively suppress the negative samples during MIL training. To address this, we calculate the negative loss, denoted as  $L_{neg}$ , which constitutes the negative component of the focal loss. The calculation is as follows, with  $\gamma$  set to 2, based on the set  $N_j$ .

$$S_p = \sigma_1(fc^{cls}(\mathbf{F}_p)) \in \mathbb{R}^K; \\ \mathcal{L}_{neg} = \frac{1}{8 * M} \sum_{j=1}^M \sum_{p \in N_j} S_p^\gamma \cdot \log(1 - S_p). \quad (12)$$

**Mask Quality Assessment.** By assimilating location and category information from annotated points, the Inspector Module gains classification capability. This allows for the prediction of semantic information, enhancing its quality assessment of the mask. Additionally, the classification scores of the marginal points (*i.e.*, negative bag) are taken into account and integrated to derive the semantic score of the mask:

$$S_{smt} = \alpha_1 \cdot mask^{cls} - \alpha_2 \cdot mask_{margin}^{cls}, \quad (13)$$

where,  $mask^{cls}$  represents the mean of classification scores across all pixels within the mask that pertain to the identical class as the annotated point. Similarly, the computation of  $mask_{margin}$  follows a akin approach.

We enhance the mask selection process by incorporating mask-associated scores with the center of mass deviation penalty introduced by the Constrainer Module. This results in a comprehensive weighted average score, derived from three quantified scores, which surpasses the performance achieved by using mask-associated scores alone.

$$Score = S_{mask} - \beta_1 \cdot S_{offset} + \beta_2 \cdot S_{smt}, \quad (14)$$

where  $S_{mask}$  is accompanied by its inherent properties at the moment of its generation given by SAM,  $S_{offset}$  is defined in Constrainer Module.

During the testing phase, we straightforwardly select the mask with the highest score as the object’s mask, which is subsequently converted into a rotated bounding box.

### 3.3 SYMMETRY AXIS ESTIMATION.

Symmetry Axis Estimation (SAE) Module primarily addresses a specific yet prevalent issue. In the case of a symmetrical object, its symmetry axes are typically considered as its orientation. As we are aware, rotated bounding boxes offer a more precise means of annotation and can also convey its orientation. Generally, an object’s orientation aligns with at least one edge of the minimum circumscribed rectangle. However, this isn’t always the case. For instance, consider an object like a plane; even though it possesses an axis of symmetry, its smallest enclosing rectangle does not have any edges parallel to its orientation, as shown in the last column of Fig. 1.

**Symmetry Axis Direction.** Assuming the presence of a symmetric object, let’s denote all its pixel coordinates as  $P$ , which forms an  $n \times 2$  matrix. By translating its center of mass to the origin, we ensure that the origin always coincides with its symmetric axis. We assert that *the eigenvectors of the matrix  $P^T \cdot P$  correspond to the object’s symmetry and vertical directions.*

**Proof of The Assertion.** In accordance with this condition, if the target exhibits symmetry along an axis passing through the origin, then there exists a rotation matrix, also referred to as an orthogonal matrix  $R$ , such that:

$$P \cdot E = Q \cdot R, E = \begin{pmatrix} 1 & 0 \\ 0 & 1 \end{pmatrix}. \quad (15)$$

Here, we have a matrix  $R$  with dimensions  $2 \times 2$ , representing a rotated matrix that aligns the axis of symmetry with the x-axis. Consequently, we can express  $Q$  as follows:

$$Q = \begin{pmatrix} x_1 & x_1 & \dots & x_n & x_n \\ y_1 & -y_1 & \dots & y_n & -y_n \end{pmatrix}^T. \quad (16)$$

To find the matrix  $R$ , we multiply both sides of the above equation by its transpose, yielding:

$$E^T \cdot P^T \cdot P \cdot E = R^T \cdot Q^T \cdot Q \cdot R. \quad (17)$$

This further simplifies to:

$$P^T \cdot P = R^T \cdot \begin{pmatrix} 2 \times \sum_{i=1}^n x_i^2 & 0 \\ 0 & 2 \times \sum_{i=1}^n y_i^2 \end{pmatrix} \cdot R. \quad (18)$$

By spectral theorem for symmetric matrices, Eq. 18 demonstrates that  $Q^T \cdot Q$  and  $P^T \cdot P$  are similar matrices, with  $R$  serving as the similarity transformation matrix and also the eigenvector matrix of  $P^T \cdot P$  because  $Q^T \cdot Q$  being a diagonal matrix. This confirms our assertion: The eigenvectors of the matrix  $P^T \cdot P$  correspond to the object’s symmetry direction and its vertical direction.

In the SAE Module, we generate oriented bounding rectangles for categories PL and HC, following their symmetry axes. For simplicity, other categories continue to use minimum circumscribed bounding boxes.

## 4 EXPERIMENTS

To evaluate our proposed method, we conduct extensive experiments on the most widely-used oriented object detection datasets, namely DOTA (Xia et al., 2018).

### 4.1 DATASETS AND IMPLEMENT DETAILS

**DOTA.** There are 2,806 aerial images—1,411 for training, 937 for validation, and 458 for testing, as annotated using 15 categories with 188,282 instances in total. We follow the preprocessing in MMRotate—The high-resolution images are split into  $1,024 \times 1,024$  patches with an overlap of 200 pixels for training, and the detection results of all patches are merged to evaluate the performance. We use training and validation sets for training and the test set for testing. The detection performance is obtained by submitting testing results to DOTA’s evaluation server. We report the  $AP_{50}$  which uses the IoU between the predicted rotated boxes and rotated ground-truth bounding boxes.

**Training Details.** P2RBox predicts the rotated bounding boxes from single point annotations and uses the predicted boxes to train three classic oriented detectors (RetinaNet, FCOS, Oriented R-CNN) with standard settings. All the fully-supervised models are trained based on a single GeForce

RTX 2080Ti GPU. Our model is trained with SGD (Bottou, 2012) on a single GeForce RTX 2080Ti GPU. The initial learning rate is  $2.5 \times 10^{-3}$  with momentum 0.9 and weight decay being 0.0001. And the learning rate will warm up for 500 iterations.

## 4.2 MAIN RESULT

Table 1: Results of each category on the DOTA-v1.0 test set.

Method	PL	BD	BR	GTF	SV	LV	SH	TC	BC	ST	SBF	RA	HA	SP	HC	mAP <sub>50</sub>
<i>Rbox-supervised:</i>																
RetinaNet (2017)	89.1	74.5	44.7	72.2	71.8	63.6	74.9	90.8	78.7	80.6	50.5	59.2	62.9	64.4	39.7	67.83
FOCS (2019)	88.4	75.6	48.0	60.1	79.8	77.8	86.7	90.1	78.2	85.0	52.8	66.3	64.5	68.3	40.3	70.78
Oriented R-CNN (2021)	89.5	82.1	54.8	70.9	78.9	83.0	88.2	90.9	87.5	84.7	64.0	67.7	74.9	68.8	52.3	75.87
RepPoints (2019b)	84.8	73.4	40.7	56.5	71.6	52.2	73.4	90.6	76.3	85.2	58.8	61.4	54.9	64.4	18.6	64.18
Faster R-CNN (2015)	88.4	73.1	44.9	59.1	73.3	71.5	77.1	90.8	78.9	83.9	48.6	63.0	62.2	64.9	56.2	69.05
RoI Transformer (2019)	88.6	78.5	43.4	75.9	68.8	73.7	83.6	90.7	77.3	81.5	58.4	53.5	62.8	58.9	47.7	69.56
DAL (2021)	88.7	76.6	45.1	66.8	67.0	76.8	79.7	90.8	79.5	78.5	57.7	62.3	69.1	73.1	60.1	71.44
RSDet (2021)	89.8	82.9	48.6	65.2	69.5	70.1	70.2	90.5	85.6	83.4	62.5	63.9	65.6	67.2	68.0	72.20
R <sup>3</sup> Det (2021b)	88.8	83.1	50.9	67.3	76.2	80.4	86.7	90.8	84.7	83.2	62.0	61.4	66.9	70.6	53.9	73.79
<i>Hbox-supervised:</i>																
BoxInst-RBox (2021)	68.4	40.8	33.1	32.3	46.9	55.4	56.6	79.5	66.8	82.1	41.2	52.8	52.8	65.0	30.0	53.59
H2RBox (2022a)	88.5	73.5	40.8	56.9	77.5	65.4	77.9	90.9	83.2	85.3	55.3	62.9	52.4	63.6	43.3	67.82
H2RBox-v2 (2023)	89.0	74.4	50.0	60.5	79.8	75.3	86.9	90.9	85.1	85.0	59.2	63.2	65.2	70.5	49.7	72.31
<i>Point-supervised:</i>																
P2BNet-H2RBox	2.3	33.8	1.2	3.6	36.7	10.2	22.3	0.2	1.6	24.5	9.1	44.4	10.5	34.8	20.9	17.08
SAM (RetinaNet)	79.7	64.6	11.1	45.6	67.9	47.7	74.6	81.1	6.6	75.7	20.0	30.6	36.9	50.5	26.1	47.91
SAM (FCOS)	78.2	61.7	11.7	45.1	68.7	64.8	78.6	80.9	5.0	77.0	16.1	31.8	45.7	53.4	44.2	50.84
SAM (Oriented R-CNN)	79.0	62.6	8.6	55.8	68.4	67.3	77.2	79.5	4.4	77.1	26.9	28.8	49.2	55.2	51.3	52.75
<b>P2RBox</b> (RetinaNet)	86.9	70.0	12.5	47.9	70.4	53.9	75.4	88.8	44.1	77.4	41.9	33.4	41.2	53.9	34.8	55.50
<b>P2RBox</b> (FCOS)	86.7	66.0	14.5	47.4	72.4	71.3	78.6	89.7	45.8	79.6	44.6	34.8	48.4	55.4	40.8	58.40
<b>P2RBox</b> (Oriented R-CNN)	87.7	72.6	13.9	63.1	70.1	74.7	82.8	90.1	46.4	81.8	53.0	33.5	57.2	56.4	50.1	62.26

As shown in Tab.1, our model’s performance across many categories is astonishing. In point-supervised detection, to demonstrate the effectiveness of the proposed method in our model, we designed a parameter-free rotation box annotation generator based on SAM, which directly retains the highest-score mask and computes the minimum bounding rectangle to obtain the rotated bounding box. By comparing the results of pseudo-label training on three strong supervised detectors, P2RBox model outperforms our baseline in every single category combined with any detector (55.50% vs. 47.91% on RetinaNet, 58.40% vs. 50.84% on FCOS, 62.26% vs. 52.75% on Oriented R-CNN).

Our mAP<sub>50</sub> is 62.26% combined with Oriented R-CNN, which exceeds the previous methods with the H2Rbox-based detector, e.g., BoxInst-RBox (Tian et al., 2021). Compared with the H2Rbox, P2RBox (Oriented R-CNN) achieves comparable performance in some categories, such as GTF and HC. Examples of detection results on the DOTA dataset using P2RBox (Oriented R-CNN) are shown in Fig. 3

## 4.3 ABLATION STUDY

The ablation study’s mAP results are based on P2RBox (RetinaNet), mIoU results are calculated between ground truth and pseudo rotated box. The following experiments assume that  $\alpha_1 = \alpha_2 = \beta_1 = \beta_2 = 1.0$  and the SAE method is applied on PL and HC if not specified.

**P2RBox Modules.** As depicted in Tab. 2, we evaluated various strategies of the P2RBox model, including Inspector Module, Constrainer Module, and the Symmetry Axis Estimation Module. Our experiments reveal the following: The first row of Tab. 2 indicates that we have confidence in the score provided by SAM for selecting the highest-scoring mask proposal. Then, we transform this mask proposal into a rotated box by calculating its minimum bounding rectangle, resulting in an mAP of 47.91%. Subsequent experiments demonstrate the performance improvements achieved by each module.

**Assessment Score.** Our mask assessment score consists of three weighted quantified scores in Eq. 14. The weight parameter  $\beta_1, \beta_2$  is used to get the final score for selecting. As shown in Tab. 3, our model demonstrates insensitivity to parameter adjustments, showing robustness.



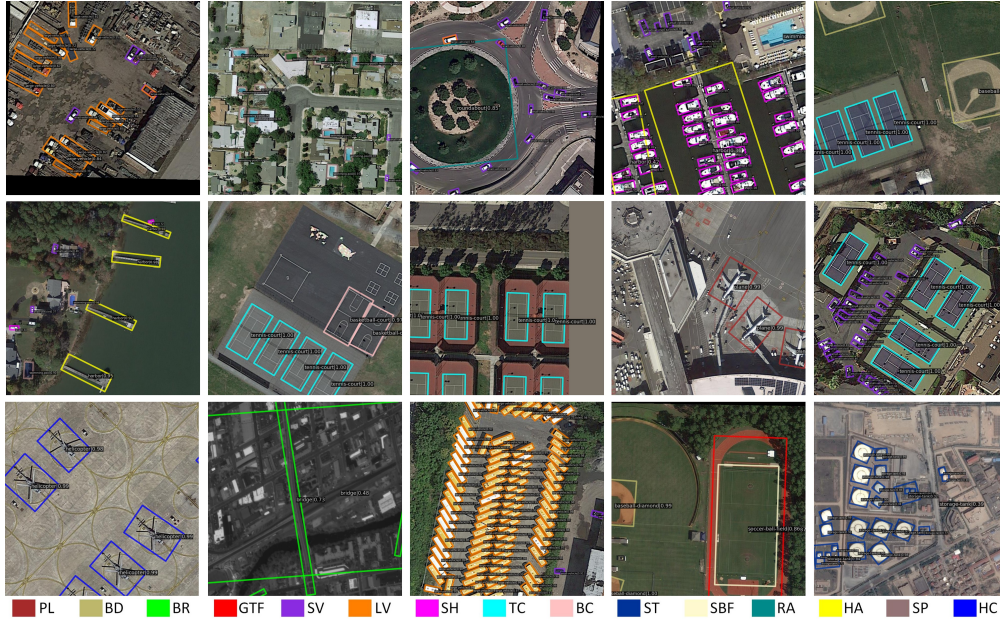


Figure 3: Examples of detection results on the DOTA dataset using P2RBox (Oriented R-CNN).

**Semantic Score.** In the Inspector Module, to harness the full potential of the network’s semantic capabilities, we conducted experiments concerning the parameters  $\alpha_1$  and  $\alpha_2$ . As demonstrated in Tab. 4, when we set  $\alpha_2 = 0$ , the mIoU decreases from 60.68% to 57.90%, when set  $\alpha_1 = 0$ , the mIoU decreases from 60.68% to 52.74%. This indicates that the model possesses the ability to distinguish between the margin and inner pixels. The subsequent experiments demonstrate that the mIoU is not significantly affected, and it is acceptable to set  $\alpha_1 = \alpha_2 = 1.0$ .

**SAE Method.** To show the full performance of SAE method, in major categories. As shown in Tab. 5, our SAE method exhibits significant improvements compared with minimum bounding rectangle in both plane (PL) and helicopter (HC), while keeping other categories basically the same.

Table 2: Ablation with main modules. Ins for Inspector, Cons for Constrainer.

Table 3: Varying  $\beta_1, \beta_2$  for assessment score.

Table 4: Varying  $\alpha_1, \alpha_2$  for semantic score.

Ins	Cons	SAE	mIoU	mAP	$\beta_1$	$\beta_2$	mIoU	$\alpha_1$	$\alpha_2$	mIoU
-	-	-	54.86	47.91	1.2	1.2	60.69	1.2	1.2	60.44
✓	-	-	55.98	49.33	1	1	60.68	1	1	60.68
-	✓	-	58.77	53.49	0.8	0.8	60.64	0.8	0.8	60.87
✓	✓	-	59.68	54.38	1.2	0.8	60.62	1.2	0.8	60.49
✓	✓	✓	60.68	55.50	0.8	1.2	60.13	0.8	1.2	59.29

Table 5: IoU results in major categories on DOTA using different methods.

Method	PL	BR	SV	LV	SH	BC	SBF	HA	HC
minimum-only	57.85	22.01	65.42	69.22	67.97	44.80	66.95	57.30	57.77
SAE-only	71.22	21.80	65.46	69.12	68.15	43.80	64.91	57.42	59.54

## 5 CONCLUSION

This paper introduces P2RBox, the first point-supervised oriented object detector to our best knowledge. P2RBox distinguishes features through multi-instance learning, introduces a novel method for assessing proposal masks, designs a SAE Module for oriented bounding box conversion, and trains a fully supervised detector. P2RBox achieves impressive detection accuracy, with the exception of complex categories like BR. P2RBox offers a training paradigm that can be based on any proposal generator, and its generated rotated bounding box annotations can be used to train various strong supervised detectors, making it highly versatile and performance-adaptive without the need for additional parameters.

## REFERENCES

- Hakan Bilen and Andrea Vedaldi. Weakly supervised deep detection networks. In *Proceedings of the IEEE conference on computer vision and pattern recognition*, pp. 2846–2854, 2016.
- Léon Bottou. Stochastic gradient descent tricks. In *Neural Networks: Tricks of the Trade: Second Edition*, pp. 421–436. Springer, 2012.
- Pengfei Chen, Xuehui Yu, Xumeng Han, Najmul Hassan, Kai Wang, Jiachen Li, Jian Zhao, Humphrey Shi, Zhenjun Han, and Qixiang Ye. Point-to-box network for accurate object detection via single point supervision. In *European Conference on Computer Vision*, pp. 51–67. Springer, 2022.
- Ze Chen, Zhihang Fu, Rongxin Jiang, Yaowu Chen, and Xian-Sheng Hua. Slv: Spatial likelihood voting for weakly supervised object detection. In *Proceedings of the IEEE/CVF Conference on Computer Vision and Pattern Recognition*, pp. 12995–13004, 2020.
- Bowen Cheng, Omkar Parkhi, and Alexander Kirillov. Pointly-supervised instance segmentation. In *Proceedings of the IEEE/CVF Conference on Computer Vision and Pattern Recognition*, pp. 2617–2626, 2022.
- Ali Diba, Vivek Sharma, Ali Pazandeh, Hamed Pirsiavash, and Luc Van Gool. Weakly supervised cascaded convolutional networks. In *Proceedings of the IEEE conference on computer vision and pattern recognition*, pp. 914–922, 2017.
- Jian Ding, Nan Xue, Yang Long, Gui-Song Xia, and Qikai Lu. Learning roi transformer for oriented object detection in aerial images. In *Proceedings of the IEEE/CVF Conference on Computer Vision and Pattern Recognition*, pp. 2849–2858, 2019.
- Mark Everingham, Luc Van Gool, Christopher KI Williams, John Winn, and Andrew Zisserman. The pascal visual object classes (voc) challenge. *International journal of computer vision*, 88: 303–338, 2010.
- Jiaming Han, Jian Ding, Jie Li, and Gui-Song Xia. Align deep features for oriented object detection. *IEEE Transactions on Geoscience and Remote Sensing*, 60:1–11, 2021a.
- Jiaming Han, Jian Ding, Nan Xue, and Gui-Song Xia. Redet: A rotation-equivariant detector for aerial object detection. In *Proceedings of the IEEE Conference on Computer Vision and Pattern Recognition*, pp. 2786–2795, 2021b.
- Shitian He, Huanxin Zou, Yingqian Wang, Boyang Li, Xu Cao, and Ning Jing. Learning remote sensing object detection with single point supervision. *arXiv preprint arXiv:2305.14141*, 2023.
- Liping Hou, Ke Lu, Xue Yang, Yuqiu Li, and Jian Xue. G-rep: Gaussian representation for arbitrary-oriented object detection. *Remote Sensing*, 15(3):757, 2023.
- Alexander Kirillov, Eric Mintun, Nikhila Ravi, Hanzi Mao, Chloe Rolland, Laura Gustafson, Tete Xiao, Spencer Whitehead, Alexander C Berg, Wan-Yen Lo, et al. Segment anything. *arXiv preprint arXiv:2304.02643*, 2023.
- Pilhyeon Lee and Hyeran Byun. Learning action completeness from points for weakly-supervised temporal action localization. In *Proceedings of the IEEE/CVF International Conference on Computer Vision*, pp. 13648–13657, 2021.
- Wentong Li, Yijie Chen, Kaixuan Hu, and Jianke Zhu. Oriented reppoints for aerial object detection. In *Proceedings of the IEEE Conference on Computer Vision and Pattern Recognition*, pp. 1829–1838, 2022.
- Tsung-Yi Lin, Priya Goyal, Ross Girshick, Kaiming He, and Piotr Dollár. Focal loss for dense object detection. In *Proceedings of the IEEE International Conference on Computer Vision*, pp. 2980–2988, 2017.
- Qi Ming, Zhiqiang Zhou, Lingjuan Miao, Hongwei Zhang, and Linhao Li. Dynamic anchor learning for arbitrary-oriented object detection. In *Proceedings of the AAAI Conference on Artificial Intelligence*, volume 35, pp. 2355–2363, 2021.

- Dim P Papadopoulos, Jasper RR Uijlings, Frank Keller, and Vittorio Ferrari. Training object class detectors with click supervision. In *Proceedings of the IEEE Conference on Computer Vision and Pattern Recognition*, pp. 6374–6383, 2017.
- Wen Qian, Xue Yang, Silong Peng, Junchi Yan, and Yue Guo. Learning modulated loss for rotated object detection. In *Proceedings of the AAAI conference on artificial intelligence*, volume 35, pp. 2458–2466, 2021.
- Shaoqing Ren, Kaiming He, Ross Girshick, and Jian Sun. Faster r-cnn: Towards real-time object detection with region proposal networks. In *Advances in Neural Information Processing Systems*, pp. 91–99, 2015.
- Zhongzheng Ren, Zhiding Yu, Xiaodong Yang, Ming-Yu Liu, Alexander G Schwing, and Jan Kautz. Ufo 2: A unified framework towards omni-supervised object detection. In *European conference on computer vision*, pp. 288–313. Springer, 2020.
- Javier Ribera, David Guera, Yuhao Chen, and Edward J Delp. Locating objects without bounding boxes. In *Proceedings of the IEEE/CVF Conference on Computer Vision and Pattern Recognition*, pp. 6479–6489, 2019.
- Qingyu Song, Changan Wang, Zhengkai Jiang, Yabiao Wang, Ying Tai, Chengjie Wang, Jilin Li, Feiyue Huang, and Yang Wu. Rethinking counting and localization in crowds: A purely point-based framework. In *Proceedings of the IEEE/CVF International Conference on Computer Vision*, pp. 3365–3374, 2021.
- Peng Tang, Xinggang Wang, Xiang Bai, and Wenyu Liu. Multiple instance detection network with online instance classifier refinement. In *Proceedings of the IEEE conference on computer vision and pattern recognition*, pp. 2843–2851, 2017.
- Peng Tang, Xinggang Wang, Song Bai, Wei Shen, Xiang Bai, Wenyu Liu, and Alan Yuille. Pcl: Proposal cluster learning for weakly supervised object detection. *IEEE transactions on pattern analysis and machine intelligence*, 42(1):176–191, 2018.
- Zhi Tian, Chunhua Shen, Hao Chen, and Tong He. Fcos: Fully convolutional one-stage object detection. In *Proceedings of the IEEE International Conference on Computer Vision*, pp. 9627–9636, 2019.
- Zhi Tian, Chunhua Shen, Xinlong Wang, and Hao Chen. Boxinst: High-performance instance segmentation with box annotations. In *Proceedings of the IEEE Conference on Computer Vision and Pattern Recognition*, pp. 5443–5452, 2021.
- Fang Wan, Pengxu Wei, Jianbin Jiao, Zhenjun Han, and Qixiang Ye. Min-entropy latent model for weakly supervised object detection. In *Proceedings of the IEEE conference on computer vision and pattern recognition*, pp. 1297–1306, 2018.
- Gui-Song Xia, Xiang Bai, Jian Ding, Zhen Zhu, Serge Belongie, Jiebo Luo, Mihai Datcu, Marcello Pelillo, and Liangpei Zhang. Dota: A large-scale dataset for object detection in aerial images. In *Proceedings of the IEEE Conference on Computer Vision and Pattern Recognition*, pp. 3974–3983, 2018.
- Xingxing Xie, Gong Cheng, Jiabao Wang, Xiwen Yao, and Junwei Han. Oriented r-cnn for object detection. In *Proceedings of the IEEE/CVF international conference on computer vision*, pp. 3520–3529, 2021.
- Xue Yang and Junchi Yan. Arbitrary-oriented object detection with circular smooth label. In *European Conference on Computer Vision*, pp. 677–694, 2020.
- Xue Yang, Jirui Yang, Junchi Yan, Yue Zhang, Tengfei Zhang, Zhi Guo, Xian Sun, and Kun Fu. Serdet: Towards more robust detection for small, cluttered and rotated objects. In *Proceedings of the IEEE International Conference on Computer Vision*, pp. 8232–8241, 2019a.
- Xue Yang, Liping Hou, Yue Zhou, Wentao Wang, and Junchi Yan. Dense label encoding for boundary discontinuity free rotation detection. In *Proceedings of the IEEE Conference on Computer Vision and Pattern Recognition*, pp. 15819–15829, 2021a.

- Xue Yang, Junchi Yan, Ziming Feng, and Tao He. R3det: Refined single-stage detector with feature refinement for rotating object. In *Proceedings of the AAAI Conference on Artificial Intelligence*, volume 35, pp. 3163–3171, 2021b.
- Xue Yang, Junchi Yan, Qi Ming, Wentao Wang, Xiaopeng Zhang, and Qi Tian. Rethinking rotated object detection with gaussian wasserstein distance loss. In *International Conference on Machine Learning*, pp. 11830–11841. PMLR, 2021c.
- Xue Yang, Xiaojiang Yang, Jirui Yang, Qi Ming, Wentao Wang, Qi Tian, and Junchi Yan. Learning high-precision bounding box for rotated object detection via kullback-leibler divergence. *Advances in Neural Information Processing Systems*, 34:18381–18394, 2021d.
- Xue Yang, Gefan Zhang, Wentong Li, Xuehui Wang, Yue Zhou, and Junchi Yan. H2rbox: Horizontal box annotation is all you need for oriented object detection. *arXiv preprint arXiv:2210.06742*, 2022a.
- Xue Yang, Gefan Zhang, Xiaojiang Yang, Yue Zhou, Wentao Wang, Jin Tang, Tao He, and Junchi Yan. Detecting rotated objects as gaussian distributions and its 3-d generalization. *IEEE Transactions on Pattern Analysis and Machine Intelligence*, 2022b.
- Xue Yang, Yue Zhou, Gefan Zhang, Jirui Yang, Wentao Wang, Junchi Yan, Xiaopeng Zhang, and Qi Tian. The kfiou loss for rotated object detection. *arXiv preprint arXiv:2201.12558*, 2022c.
- Ze Yang, Shaohui Liu, Han Hu, Liwei Wang, and Stephen Lin. Reppoints: Point set representation for object detection. In *Proceedings of the IEEE/CVF international conference on computer vision*, pp. 9657–9666, 2019b.
- Xuehui Yu, Pengfei Chen, Di Wu, Najmul Hassan, Guorong Li, Junchi Yan, Humphrey Shi, Qixiang Ye, and Zhenjun Han. Object localization under single coarse point supervision. In *Proceedings of the IEEE/CVF Conference on Computer Vision and Pattern Recognition*, pp. 4868–4877, 2022.
- Yi Yu and Feipeng Da. Phase-shifting coder: Predicting accurate orientation in oriented object detection. In *Proceedings of the IEEE/CVF Conference on Computer Vision and Pattern Recognition*, pp. 13354–13363, 2023.
- Yi Yu, Xue Yang, Qingyun Li, Yue Zhou, Gefan Zhang, Junchi Yan, and Feipeng Da. H2rbox-v2: Boosting hbox-supervised oriented object detection via symmetric learning. *arXiv preprint arXiv:2304.04403*, 2023.
- Xiaolin Zhang, Yunchao Wei, Jiashi Feng, Yi Yang, and Thomas S Huang. Adversarial complementary learning for weakly supervised object localization. In *Proceedings of the IEEE conference on computer vision and pattern recognition*, pp. 1325–1334, 2018.
- Bolei Zhou, Aditya Khosla, Agata Lapedriza, Aude Oliva, and Antonio Torralba. Learning deep features for discriminative localization. In *Proceedings of the IEEE conference on computer vision and pattern recognition*, pp. 2921–2929, 2016.

6 APPENDIX

**Upper Limit in our method** In fact, we don't create new mask proposals; we simply choose a mask from the SAM generator using our criteria. As a result, there's a performance limit. When selecting based on IoU with the ground truth, the IoU results are displayed in Tab. 6. This result demonstrates

Table 6: IoU result of SAM (highest score), P2RBox, ceiling (always choose the highest IoU using SAE on PL and HC while others minimum).

Method	PL	BD	BR	GTF	SV	LV	SH	TC	BC	ST	SBF	RA	HA	SP	HC	mIoU
SAM	55.70	60.72	17.85	62.65	63.79	65.90	67.06	78.38	25.54	57.87	46.12	48.47	52.26	60.20	56.04	54.57
P2RBox	71.22	66.10	22.01	64.83	65.42	69.22	67.97	80.70	44.80	58.49	66.95	52.22	57.30	63.50	59.54	60.68
IoU-highest	74.08	70.39	26.23	78.53	69.61	73.48	74.91	83.43	47.14	64.61	70.08	58.37	66.51	66.81	64.11	65.89

that we have outperformed the SAM model in every category compared to simply selecting the highest score. It also highlights that for some categories, the performance remains poor due to very low upper limits, despite significant improvements from the baseline.

**Details when using Symmetry Axis Estimation Module.** Tab. 7 provides detailed information. The SAE method shows a slight decrease in IoU for some categories, which is negligible. However, it experiences a significant drop in the BD category. The issue arises because the annotation or

Table 7: Different mask2rbox method IoU results.

Method	PL	BD	BR	GTF	SV	LV	SH	TC	BC	ST	SBF	RA	HA	SP	HC	mIoU
minimum-only	57.85	66.10	22.01	64.83	65.42	69.22	67.97	80.70	44.80	58.49	66.95	52.22	57.30	63.50	57.77	59.68
SAE-only	71.22	58.14	21.80	64.94	65.46	69.12	68.15	80.37	43.80	56.00	64.91	52.87	57.42	62.95	59.54	59.78

ground truth for BD does not align with its symmetry axis, even when a symmetry axis is present, as illustrated in Fig. 4.

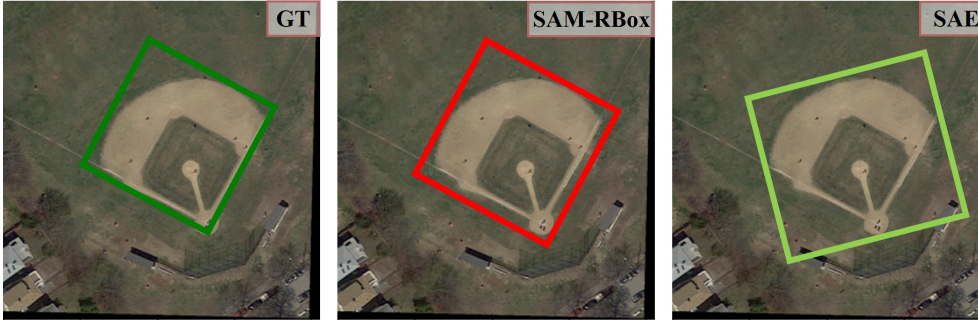


Figure 4: GT, minimum and SAE on category BD.

**The limitations on the upper performance bound for the Bridges.** category are quite restrictive. This is primarily attributed to the distinctive nature of its definition, which deviates from the conventional object definitions. In the case of bridges, they are defined as road segments that span across bodies of water, leading to a situation where there are insufficient discernible pixel variations between the left and right ends of the bridge. Consequently, this characteristic significantly hampers the performance of the SAM model. As a result, it imposes a notable constraint on the potential performance within this category. This challenge is further exemplified in Fig. 5.

**Details in Inspector Module.** We designed the coefficients of the Inspector Module to address challenges posed by small-scale objects. In cases where a small-scale object assimilates excessive background context, the increment in the denominator term *Radius* within the coefficient formulation leads to a reduction in the *S<sub>offset</sub>*. Consequently, as shown in Fig. 6 this deviation in *S<sub>offset</sub>* guides the bias observed in our selection of outcomes.

**What Result in Bad Bases using minimum bounding rectangle.** To illustrate this without loss of generality, let's consider an object that exhibits symmetry about the y-axis (see Fig. 7). We'll denote three points on the oriented circumscribed bounding box as *a*, *b*, and *c*, respectively, and their corresponding mirror points as  $\hat{a}$ ,  $\hat{b}$ , and  $\hat{c}$ .



Figure 5: Category BR, with mask proposals generated by SAM with annotated point and its circumscribed rbox.

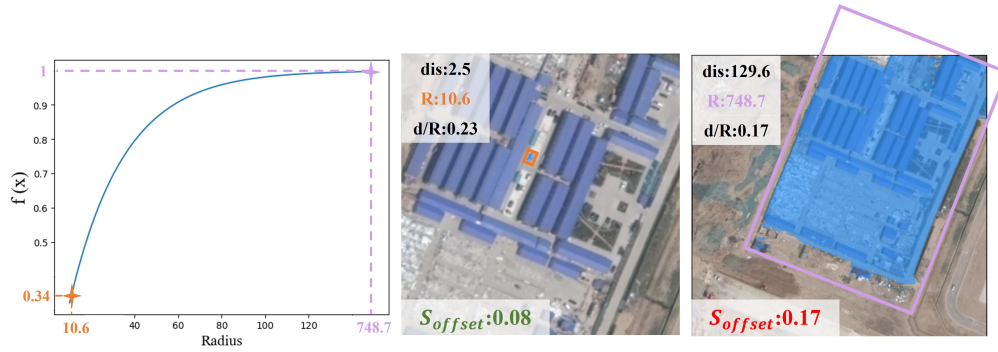


Figure 6: The influence of the coefficients of the Inspector Module.

Now, suppose there exists a minimum circumscribed bounding box, denoted as  $Mbox$ , which is distinct from  $Rbox$ . By virtue of symmetry,  $Mbox$  must also exhibit symmetry, compelling its shape to be square with its diagonal aligned along the axis of symmetry. To encompass the entire object,  $Mbox$  must enclose points  $a$ ,  $b$ , and  $c$  as illustrated in Fig. 7 (a). Let  $d$  represent the length of the diagonal of  $Mbox$ . We have the following conditions:

$$d \geq \max(h + x_a, w/2 + y_b) - \min(-x_c, y_b - w/2), \quad (19)$$

$$d^2 \leq 2 \times w \cdot h. \quad (20)$$

The second inequality is derived based on the area requirement. For the more general case, as shown in Fig. 7 (b). By finding two tangent lines with fixed slopes (1 and -1), where  $\alpha \cdot h$  is the distance between the intersections of these lines with the right green edge, we obtain an equation regarding the length of the diagonal:

$$d = w + \alpha \cdot h. \quad (21)$$

Specifically, if the width is equal to the height,  $w = h$ , the inequality simplifies to:

$$\alpha \leq \sqrt{2} - 1. \quad (22)$$

In conclusion, taking an airplane as an example, as shown in the last column of Fig. 1, due to the intersection ratio  $\alpha < \sqrt{2} - 1$ , ambiguity arises between the minimum bounding rectangle and the oriented bounding rectangle, which is well addressed by Symmetry Axis Estimation Module.

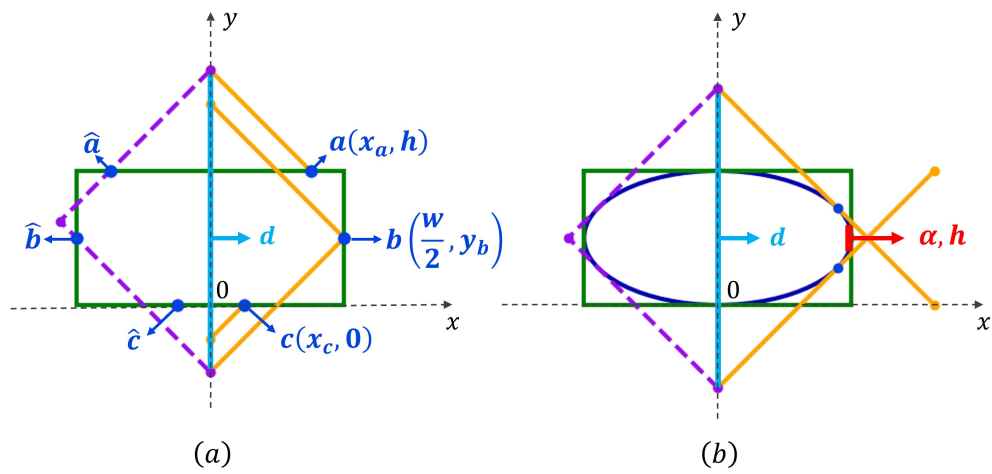


Figure 7: Convex polygon example compared to the general case.